Estimating Signal-to-Clutter Ratio of InSAR Corner Reflectors From SAR Time Series

Richard Czikhardt, Hans van der Marel, Freek J. van Leijen, *Member, IEEE*, and Ramon F. Hanssen, *Senior Member, IEEE*

***Abstract*— The estimation of Signal-to-Clutter Ratio (SCR) of a radar point target, such as a corner reflector, is an essential step for synthetic aperture radar (SAR) interferometry and positioning, as it influences the phase measurement variance as well as the absolute positioning precision. The standard method to estimate the SCR of a point target relies on the debatable assumption of spatial ergodicity, using the clutter of the surrounding as representative of the clutter at the point target. Here, we estimate the SCR of a corner reflector using a time series of SAR measurements, i.e., assuming temporal ergodicity. This assumption is often more realistic, particularly in a complex environment, in the presence of other point scatterers, and for small-sized reflectors. Empirical results on a corner reflector network, using Sentinel-1 SAR measurements, show that the temporal method yields a less biased and more precise estimate of the average SCR. A second experiment shows that the InSAR phase variance as well as positioning precision, predicted using SCR estimated by the temporal estimation method, is closer to the truth.**

***Index Terms*— Corner reflector (CR), radar-cross-section (RCS), signal-to-clutter ratio (SCR), synthetic aperture radar (SAR), SAR interferometry (InSAR), SAR positioning, InSAR phase variance.**

I. Introduction

CORNER reflectors are commonly used for radiometric and geometric synthetic aperture radar (SAR) sensor calibration and validation, [1]–[3], SAR interferometry (InSAR) applications over areas with few natural coherent reflectors [4], and for InSAR datum connection and geodetic integration [5].

These methods require a precise and unbiased estimation of the Signal-to-Clutter Ratio (SCR): the ratio of the Radar-Cross section (RCS) of the reflector and the power of its background clutter. The SCR estimate is used to estimate the InSAR phase variance [6] and the absolute positioning accuracy [7] of point targets, such as corner reflectors, for geodetic applications.

The standard method for estimating RCS and SCR of point targets involves spatial numerical integration of pixel intensity values in square-law detected SAR images [8], [9]. It assumes that the background clutter over the integrated area exhibits the same statistical properties as its surroundings, i.e., spatial ergodicity. However, for geodetic applications using medium-resolution SAR data clutter in the surrounding pixels is often not representative and sometimes contains other point scatterers (PSs), violating the assumption of spatial ergodicity.

Here, we propose to estimate the SCR of small-to-medium-sized corner reflectors using SAR time series.

The objective is to obtain an unbiased and precise average SCR estimate under the assumption on the temporal ergodicity. SAR time series are currently in abundance thanks to the operational SAR satellite missions, such as Sentinel-1. A secondary objective of the proposed method is to utilize the time series of RCS to track the reflector performance, and identify possible outliers due to damage, debris accumulation, or other external factors.

II. Methodology

A *point scatterers* (PS) response in the SAR image is a "sinc-like" 2-D impulse response function (IRF) in azimuth and range [10]. A corner reflector is an approximation of an ideal radar PS, P. Considering single-look-complex (SLC) SAR images in the zero-Doppler geometry, the phasor measurement y_P per resolution cell R_P containing a dominant PS P consists of a real $\mathrm{Re}\{y_P\}$ and an imaginary $\mathrm{Im}\{y_P\}$ signal component

$$y_P = \mathrm{Re}\{y_P\} + j\mathrm{Im}\{y_P\} = \sum_{i \in R_P} A_i \exp(j\psi_i) \tag{1}$$

which is the coherent summation of the backscatter from the PS P and the scattering contributions of its surroundings—the clutter—within the same resolution cell R_P, where A is the amplitude and ψ the phase.

A. Radar Cross Section

The power (intensity) of the signal in (1) is $A_P^2 = \mathrm{Re}\{y_P\}^2 + \mathrm{Im}\{y_P\}^2$. The pixel intensity is stored in the SLC image as a *digital number* (DN). Scaling factors are used to express DN in terms of a specific backscattering coefficient.

In the context of PS, DN is converted to RCS, which describes the ability of a PS to intercept incident energy with an effective cross-sectional area and reflect it in the direction of a radar receiver [1]. For an idealized PS response in the absence of clutter, the RCS is the integral of the power (signal energy) under its IRF [8].

RCS is strictly related to PS. For *distributed scatterers* (DS), a dimensionless *backscattering coefficient*, σ_0, is generally used to describe their mean reflectivity per unit area of a horizontal surface. Contrary to σ_0, *radar brightness*, β_0, is independent of the radar signal's local incidence angle, as its

Manuscript received February 24, 2021; revised March 25, 2021; accepted March 28, 2021. Date of publication April 14, 2021; date of current version December 22, 2021. *(Corresponding author: Richard Czikhardt.)*

Richard Czikhardt is with the Department of Theoretical Geodesy and Geoinformatics, Slovak University of Technology, 810 05 Bratislava, Slovakia (e-mail: richard.czikhardt@stuba.sk).

Hans van der Marel, Freek J. van Leijen, and Ramon F. Hanssen are with the Department of Geoscience and Remote Sensing, Delft University of Technology, 2628 Delft, The Netherlands.

Digital Object Identifier 10.1109/LGRS.2021.3070045

area normalization is in the slant-range direction [11]. Radar brightness is computed via [12]

$$\beta_0 = \left(\mathrm{DN}^2 - \eta\right) \alpha_{\mathrm{DN}}^{-2} K^{-1} \tag{2}$$

where the calibration constant K and the pixel scaling factor α_{DN} are annotated in the metadata of SLC products. α_{DN} is given as a pixel lookup table (LUT). The thermal noise correction η, i.e., the Noise-Equivalent-Sigma-Zero (NESZ), is applied if available in the LUT annotation (e.g., in the case of Sentinel-1 data [13]). Given the local incidence angle, θ, σ_0 is readily obtained from β_0 as $\sigma_0 = \beta_0 \sin\theta$. Henceforth, we assume a dimensionless, calibrated, and noise-corrected amplitude measurement, A, obtained from (2) as $A = (\beta_0)^{1/2}$.

B. Signal-to-Clutter Ratio

DS can be considered as the coherent summation of many random elementary scatterers within a resolution cell. Therefore, the central limit theorem applies, and the probability density function (PDF) of a DS complex phasor per image pixel is circular Gaussian [14]. Consequently, its amplitude A (1) is Rayleigh distributed with [15]

$$\mathrm{PDF}(A|\sigma) = \frac{A}{\sigma^2} \exp\left[-\frac{A^2}{2\sigma^2}\right] \tag{3}$$

where σ is a scale parameter, related to the expected value of the power by $\mathbb{E}(A^2) = 2\sigma^2$, and the phase $\psi \in [-\pi, \pi)$ is uniformly distributed [16].

PS, on the other hand, can be considered a signal determined by their physical properties and coherence. However, they are typically superimposed on the surrounding scatterers within the same resolution cell, i.e., the clutter. The ratio between the signal and the clutter is described by the SCR, and is a metric for the noise in the PS. Consider a PS characterized by complex phasor y. Clutter in the same resolution cell introduces circular Gaussian noise n characterized by its expected value $\mathbb{E}(n) = 0$ and variance σ_n^2 for both its real and imaginary components. The PS amplitude A (1) follows a Rice distribution [16], [17]:

$$\mathrm{PDF}(A|\mu, \sigma_n) = \frac{A}{\sigma_n^2} I_0\left(\frac{A\mu}{\sigma_n^2}\right) \exp\left[\frac{-\left(A^2 + \mu^2\right)}{2\sigma_n^2}\right] \tag{4}$$

where I_0 is the modified-Bessel function of the first kind with order zero and $\mu = \mathbb{E}(A)$ is the expected value of the amplitude. The shape of the Rice distribution is determined by the SCR

$$\mathrm{SCR} = \frac{\mu^2}{2\sigma_n^2} \tag{5}$$

which is the ratio of a reflector's signal power to the power of the surrounding clutter within the resolution cell. Note that for clutter only, the Rice PDF transforms to a Rayleigh PDF driven solely by variance $\sigma_n^2 = \mathbb{E}(A^2)/2$.

C. Spatial SCR Estimation Method

If SAR sensor and processing gain factors are known, and DN values, see (2), are scaled to pixel intensities, the standard RCS estimation formula [8], [9] can be rewritten as [12], [18]

$$\mathrm{RCS} = \frac{I_P}{K} \frac{P_A}{C_F} \tag{6}$$

where I_P is the total (integrated) power in the mainlobe (which is not directly observable due to the superimposition with clutter occupying the same resolution cell as the point target), C_F is the relative power in the sidelobes and P_A is the sample (pixel) area. As the IRF is finitely sampled by the SAR image pixels, oversampling and numerical integration is employed within the estimation process. The components of (6) are approximated as follows:

- I_P We estimate the background clutter C from four areas (quadrants) outside the cross-shaped area of the IRF, assuming spatial ergodicity. We subtract C from all pixel intensities within a center area of 2 by 2 resolution cells (half-power width of IRF), centered at the point target. We integrate corrected pixel intensities within the center area, which yields I_P.
- C_F We estimate the sidelobe energy from pixels spanning the cross-shaped area of the IRF (excluding the center area) within 10 by 10 resolution cells. We then compute the ratio between the total energy in the sidelobes (excluding the main lobe) and the energy in the main lobe, i.e., the integrated sidelobe ratio (ISLR). The relative power in the sidelobes is $C_F = 1/(1 + \mathrm{ISLR})$.
- K calibration constant as annotated in the SLC metadata.
- P_A azimuth times slant-range pixel spacing in meters.

The SCR is obtained as the ratio of the estimated I_P and the estimated clutter power C, multiplied by the mainlobe area $\Delta_{\mathrm{mainlobe}}$

$$\mathrm{SCR} = \frac{I_P}{C \cdot \Delta_{\mathrm{mainlobe}}}. \tag{7}$$

D. Temporal SCR Estimation Method

An alternative to the spatial SCR estimation method is to compute the average SCR from the time series of the instantaneous "apparent RCS", using the *peak* method [8], [19], and maximum likelihood estimation (MLE) to estimate the mean RCS and the clutter. Defining the resolution as the half-power width (−3 dB) of the IRF main lobe, multiplying the IRF peak intensity with the resolution cell area yields the volume of a rectangular box which is the same as the power under an IRF.

The original peak method assumes that the space-averaged clutter and mean system noise are used to correct the peak response. However, the clutter power estimated from nearby pixels in medium-resolution SAR imagery in areas with spatially varying clutter may be inaccurate. Therefore, we intentionally omit this correction in the "apparent RCS" computation

$$\mathrm{RCS} \approx \beta_0 \cdot \Delta_{az} \Delta_r \quad [\mathrm{m}^2] \tag{8}$$

where $\Delta_{\mathrm{az/r}}$ are the azimuth and range resolution, respectively. Peak and clutter contributions are separated from the amplitude time series assuming temporal ergodicity. Given a reasonably large time series (>20 images), two independent clutter power estimates are obtained by:

1) a maximum likelihood fit of a Rayleigh distribution, see (3), to the amplitude time series of the site prior to the

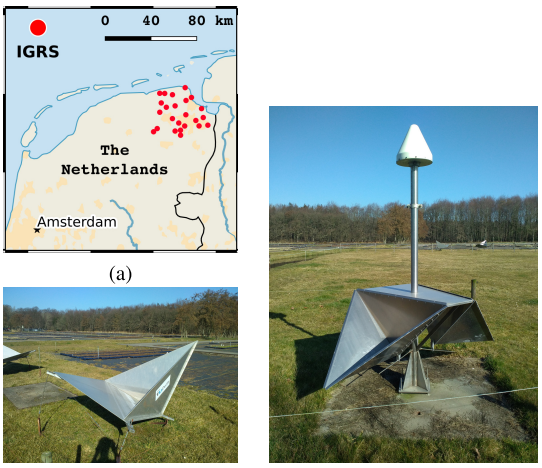

Fig. 1. (a) Network of 24 Integrated Geodetic Reference Stations. (b) CRDS reference reflector used in the second experiment. (c) Integrated Geodetic Reference Stations DBFT reflector used in both experiments.

installation of the reflector, to estimate the power of the clutter, and

2) a maximum likelihood fit of a Rice distribution to the peak amplitude time series of the reflector after installation, to separate the clutter and PS contributions via its two parameters, see (4). The first parameter, $\hat{\mu}_{\mathrm{MLE}}$, multiplied by the resolution cell area yields the reflector's RCS, see (8). The second parameter, $\hat{\sigma}_{\mathrm{MLE}}$, represents the power of the clutter while the reflector is in place (provided its statistical properties are not undergoing significant temporal changes). The ratio of the two parameters is the estimate of the SCR, see (5)

$$\hat{\mathrm{SCR}} = \frac{\hat{\mu}^2_{\mathrm{MLE}}}{2\hat{\sigma}^2_{\mathrm{MLE}}}. \tag{9}$$

Note that the sample mean and the standard deviation (STD) are biased estimators for μ and σ, although their ratio, known as the normalized amplitude dispersion, is generally used as the phase STD proxy in InSAR applications [17]. If the assumption on the stationarity of the clutter is violated, it still yields the unbiased average SCR estimate, although not fully representative for the instantaneous RCS (considering, e.g., seasonal or secular variations). Absolute radiometric calibration, however, is not the primary objective of the temporal estimation method. Potential outliers in the "apparent" RCS (e.g., due to debris accumulation) are readily handled in time series analysis using a threshold of three median absolute deviations (MAD), thus ensuring the reflector's RCS does not significantly vary in time.

III. Experiment

The viability of the proposed method is tested on Sentinel-1 C-band SLC time series in two different experiments in the Netherlands. The first experiment uses a corner reflector network with 24 sites (48 reflectors), see Fig. 1. The second experiment uses two proximate corner reflectors. For each experiment, a time series of three years with a 6-day acquisition interval is collected, from April 2017 until April 2020, including one year of measurements before installation. For

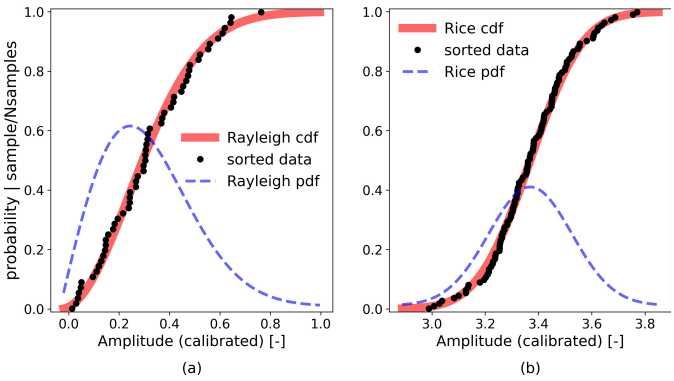

Fig. 2. Sorted and scaled amplitude data of a resolution cell before (a) and after (b) corner reflector installation, corresponding to the background clutter and the point target response, respectively. The background clutter follows a Rayleigh distribution whereas the reflector follows a Rice distribution.

each reflector, an image patch of 10×10 resolution cells is selected and oversampled by a factor 32 in the frequency domain using zero-padding. Then, we estimate the precise peak position and amplitude by fitting a 2-D elliptic paraboloid over a small image subpatch, centered at the oversampled amplitude maximum of the initial image patch [3].

A. Corner Reflector Network Experiment

Both the spatial and the temporal RCS and SCR estimation methods were applied on ascending track 88 and descending track 139 covering the network of Integrated Geodetic Reference Stations (IGRS) in Groningen, see Fig. 1(a). Each of the 24 IGRS stations consists of a global navigation satellite system (GNSS) antenna and two back-flipped triangular trihedral corner reflectors, see Fig. 1(c), with an inner edge length of 0.9 m and a corresponding theoretical RCS of 29.5 dBm^2 at bore-sight for C-band [20]. Fig. 2(a) and (b) shows the distribution of the observed radar brightness values for a particular resolution cell, before and after corner reflector installation, respectively. The corresponding distribution functions match with the Rayleigh and the Rice distribution. This sustains our assumption on the validity of these functions, see Section II-D.

Fig. 3 shows scatter plots of the temporally averaged results for all 48 reflectors. Fig. 3(a) confirms that the estimated RCS values of the reflectors by the temporal method (TM) are comparable to the spatial method (SM). The mean and STD of the differences are 0.04 and 0.42 dB, respectively. The black dots show the analytical RCS values computed using a geometric optics simulation [1], [21], taking into account the corner reflector alignment for each acquisition. Fig. 3(b) shows that the precision of the RCS estimates, expressed as the STD of the time series, is significantly better for the TM. This is mainly because the TM does not use the instantaneous clutter estimates to correct (8), whereas the SM does. The higher precision of the TM is also justified considering the reported 0.25 dB radiometric stability (1 sigma) of Sentinel-1 SLC data [2]. Fig. 3(c) shows that the differences between the spatial and TMs for SCR estimation are significant. This is caused by the different strategies of clutter estimation. While the SM uses samples outside the IRF (which represents surfaces tens to hundreds of meters away from the actual reflector

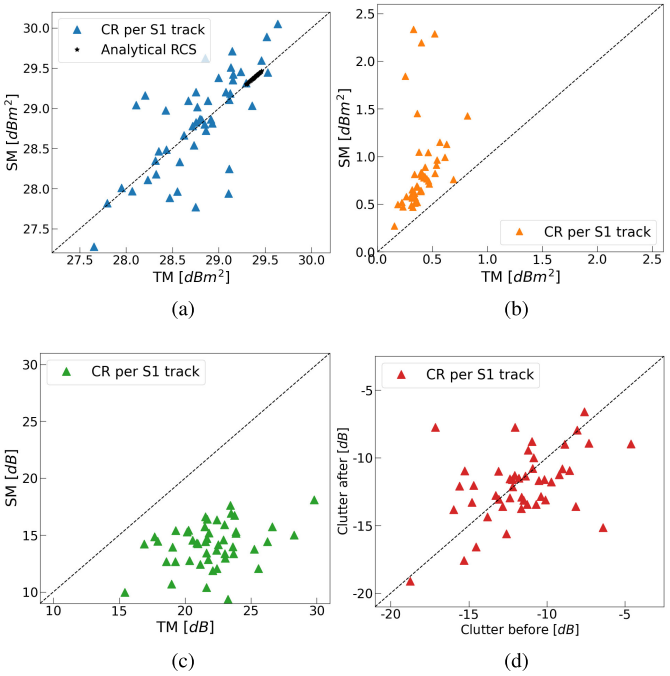

Fig. 3. (a)–(c) Comparison of the spatial method (SM) and the temporal method (TM) for RCS and SCR estimation of 48 corner reflectors (CRs) on three years of Sentinel-1 time series from ascending track 88 and descending track 139. (d) Clutter power estimated by the temporal method (TM) before/after corner reflector deployment. Each triangle represents a single CR of the network. (a) Average RCS. (b) RCS STD. (c) Average SCR. (d) Clutter power.

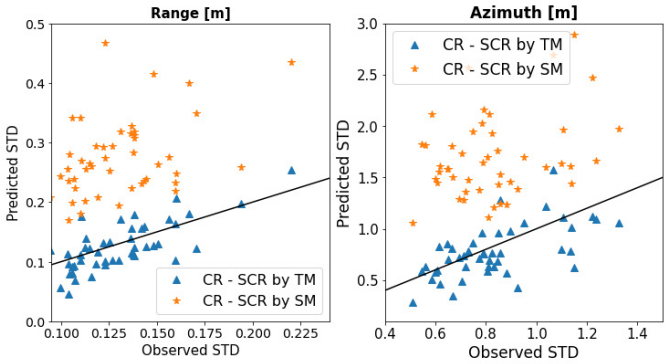

Fig. 4. Predicted versus estimated STDs (STD) of observed peak positions in azimuth and range (in meters) from a time series of 150 Sentinel-1 acquisitions. Each point represents a single corner reflector.

TABLE I
SCR-DERIVED VERSUS OBSERVED DOUBLE-DIFFERENCED PHASE STANDARD DEVIATIONS (STDS), IN MILLIMETERS

		$\sigma_{\psi}^{\mathrm{SCR}}$		$\sigma_{\Delta\phi}^{\mathrm{SCR}}$		
Track	Reflector	SM	TM	SM	TM	$\hat{\sigma}_{\Delta\phi}$
DSC t037	CRDS	0.22	0.10	1.00	0.47	0.43
	DBFT	0.67	0.32			
DSC t110	CRDS	0.21	0.11	1.13	0.47	0.44
	DBFT	0.77	0.31			

position in case of medium-resolution data), the TM uses samples directly from the reflector, albeit assuming temporal ergodicity of the SCR in the time series. Finally, Fig. 3(d) depicts an independent validation of clutter power estimates using the TM, see Section II-D. The clutter power values estimated from time series after reflector installation (Rice distribution fit, scale parameter) differ by 0.05 dB in the mean with 3.84 dB STD from the independently estimated values from the time series before reflector's deployment (Rayleigh distribution fit).

The estimated SCR can be used to predict the peak position variance in the radar coordinates (azimuth and range) [7]. We do the reverse and use the observed peak position variance to compare with the predictions computed by the spatial and the TM. The observed subpixel peak positions were corrected for the effects of reference frame motion, solid earth tides, atmospheric signal delay, and Sentinel-1 specific processor biases in both azimuth and range, as reported in [22]. Fig. 4 shows that the positioning STDs predicted by the SM are higher than the observed STDs. On the other hand, STDs predicted by the TM are equal or slightly lower. The latter is what we expect: the predicted values are the Cramer–Rao Lower Bound (CRLB) and should be smaller than those observed, and the observed STD is affected by other errors, such as variations in tropospheric signal delay, which could not be completely mitigated.

B. Short Baseline Experiment

An experiment to evaluate the bias in the estimated SCR is performed on a test site where two corner reflectors, "CRDS" and "DBFT," form a very short baseline of 102 m length. Under such circumstances, the clutter can be considered the main component of the phase variance. CRDS is a square-based trihedral, see Fig. 1(a), with an inner edge length of 1.425 m and a corresponding peak-RCS of 40.7 dBm^2 for C-band, while DBFT is a back-flipped triangular trihedral with an inner edge length of 0.9 m and a corresponding peak-RCS of 29.5 dBm^2 for C-band.

The CRLB, $\sigma_{\psi}^{\mathrm{SCR}}$, [6] of the single-epoch phase measurement ψ, computed from the estimated SCR and propagated to the double-differenced InSAR phases, $\sigma_{\Delta\phi}^{\mathrm{SCR}}$, with $\sigma^2_{\Delta\phi_{i,j}} = 2\sigma^2_{\psi_i} + 2\sigma^2_{\psi_j}$, is compared to the STD $\hat{\sigma}_{\Delta\phi}$ estimated on the actual observed double-differenced phase measurements. Results for different SCR estimation methods are shown in Table I. For the SM we used the temporally averaged SCR. The empirical STD, $\hat{\sigma}_{\Delta\phi}$, is computed from the detrended double-differenced phase measurements of two descending Sentinel-1 tracks spanning 2.5 years, i.e., 150 acquisitions, see Fig. 5. Considering the sensor noise, not accounted for by the CRLB prediction, the comparison shows that the TM provides a more realistic, unbiased phase variance prediction, hence the SCR estimate, while the SM overestimates it, even if a sizeable temporal average is used.

IV. Discussion and Conclusion

The pros and cons of the spatial and temporal SCR estimation methods for corner reflectors are summarized in Table II. The significant STD of the clutter power differences, estimated by the TM, shows that the temporal ergodicity assumption may be violated. Nonetheless, for small-sized InSAR corner

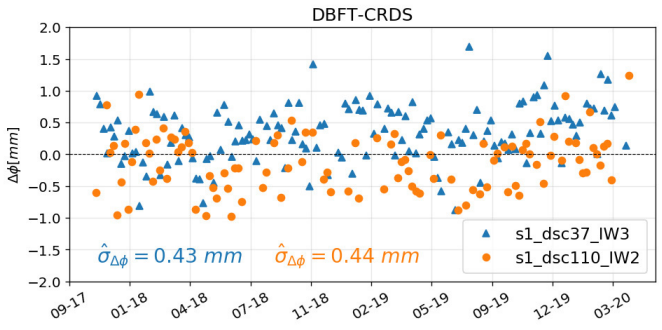

Fig. 5. Observed double-differenced phase time series between reflectors DBFT and CRDS.

TABLE II
COMPARISON OF THE SPATIAL AND THE TM FOR SCR ESTIMATION

Spatial method (SM)	Temporal method (TM)
advantages	
• Epoch-wise description of IRF • Instantaneous RCS representative of secular or seasonal effects • Invariant to resolution values	• Higher precision • Unsupervised clutter estimation • Less biased SCR estimate in a complex environment
disadvantages	
• Assumption on spatial ergodicity of the clutter • Biased SCR estimate in case of close proximity of other point scatterers or significant clutter	• Assumption on temporal ergodicity of the clutter, time series needed • Precise resolution values needed • Sidelobes not accounted for

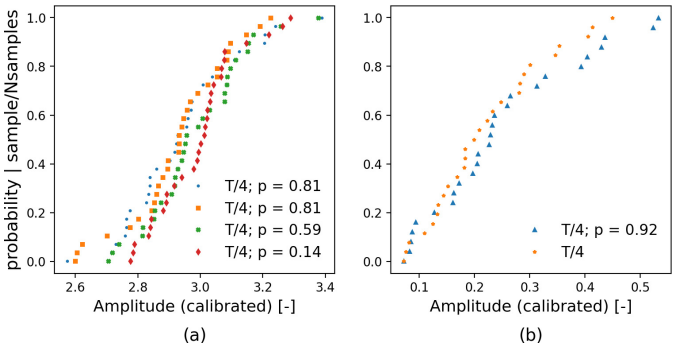

Fig. 6. Empirical distributions of quarterly temporal subsets ($T/4$, where $T = 1$ year) of the amplitude time series for DBFT reflector (a) and the corresponding background clutter observed prior to reflector deployment (b). p-values come from the Kolmogorovov–Smirnovov test (KS) 2-sample test.

reflectors with proximate PSs, this assumption is often more realistic than the assumption of spatial ergodicity. As an example, Fig. 6 shows empirical distributions of the amplitude time series for reflector DBFT split into quarterly temporal subsets, $T/4$, where $T = 1$ year. Using Kolmogorov–Smirnov 2-sample tests, we could not reject our two hypotheses that the subsets with the reflector [Fig. 6(a)] follow the same probability distribution and the subsets with the clutter [Fig. 6(b)] follow the same distribution. Moreover, the assumption of spatial ergodicity cannot be fulfilled as the surroundings of the reflectors are often not homogeneous random scatterers but may contain several other PSs. The temporal SCR estimate, invariant to the potential RCS estimate bias, is more realistic with respect to the STD of the phase measurement and positioning precision, which are imperative for InSAR applications.

REFERENCES

[1] A. W. Doerry, "Reflectors for SAR performance testing," Sandia Nat. Lab., Albuquerque, NM, USA, Tech. Rep. SAND2008-0396, Jan. 2008.
[2] *Sentinel-1A N-Cyclic Performance Report—2020-07*, Collecte Localisation Satellites (CLS), Ramonville Saint-Agne, France, Jul. 2020.
[3] U. Balss *et al.*, "Survey protocol for geometric SAR sensor analysis," German Aerospace Center (DLR), Tech. Univ. Munich (TUM), Remote Sensing Lab. Univ. Zurich, Zürich, Switzerland, Tech. Rep. DLR-FRM4SAR-TN-200, Apr. 2018.
[4] M. Garthwaite, "On the design of radar corner reflectors for deformation monitoring in multi-frequency InSAR," *Remote Sens.*, vol. 9, no. 7, p. 648, Jun. 2017.
[5] P. Mahapatra, H. V. der Marel, F. van Leijen, S. Samiei-Esfahany, R. Klees, and R. Hanssen, "InSAR datum connection using GNSS-augmented radar transponders," *J. Geodesy*, vol. 92, no. 1, pp. 21–32, Jun. 2017.
[6] P. Dheenathayalan, M. Caro Cuenca, P. Hoogeboom, and R. F. Hanssen, "Small reflectors for ground motion monitoring with InSAR," *IEEE Trans. Geosci. Remote Sens.*, vol. 55, no. 12, pp. 6703–6712, Dec. 2017.
[7] R. Bamler and M. Eineder, "Accuracy of differential shift estimation by correlation and split-bandwidth interferometry for wideband and delta-K SAR systems," *IEEE Geosci. Remote Sens. Lett.*, vol. 2, no. 2, pp. 151–155, Apr. 2005.
[8] A. L. Gray, P. W. Vachon, C. E. Livingstone, and T. I. Lukowski, "Synthetic aperture radar calibration using reference reflectors," *IEEE Trans. Geosci. Remote Sens.*, vol. 28, no. 3, pp. 374–383, May 1990.
[9] A. Freeman, "SAR calibration: An overview," *IEEE Trans. Geosci. Remote Sens.*, vol. 30, no. 6, pp. 1107–1121, Jun. 1992.
[10] R. Bamler and P. Hartl, "Synthetic aperture radar interferometry," *Inverse Problems*, vol. 14, no. 4, p. 1, 1998.
[11] R. K. Raney, T. Freeman, R. W. Hawkins, and R. Bamler, "A plea for radar brightness," in *Proc. IEEE Int. Geosci. Remote Sens. Symp.*, Aug. 1994, pp. 1090–1092.
[12] N. Miranda and P. J. Meadows, "Radiometric calibration of S-1 level-1 products generated by the S-1 IPF," European Space Agency (ESA), Paris, France, Tech. Rep. ESA-EOPG-CSCOP-TN-0002, May 2015.
[13] R. Piantanida, N. Miranda, and G. Hajduch, "Thermal denoising of products generated by the S-1 IPF," Sentinel-1 Mission Perform. Centre, Ramonville-Saint-Agne, France, Tech. Rep. MPC-0392, Nov. 2017.
[14] J. C. Dainty, *Laser Speckle Rel. Phenomena* (Topics in Applied Physics), vol. 9. Berlin, Germany: Springer-Verlag, 1975.
[15] R. F. Hanssen, *Radar Interferometry: Data Interpretation Error Analysis*, vol. 2. Dordrecht, The Netherlands: Springer, 2001.
[16] C. Oliver and S. Quegan, *Understanding Synthetic Aperture Radar Images*. Chennai, India: SciTech, 2004.
[17] A. Ferretti, C. Prati, and F. Rocca, "Permanent scatterers in SAR interferometry," *IEEE Trans. Geosci. Remote Sens.*, vol. 39, no. 1, pp. 8–20, Jan. 2001.
[18] K. Schmidt, M. Schwerdt, N. Miranda, and J. Reimann, "Radiometric comparison within the Sentinel-1 SAR constellation over a wide backscatter range," *Remote Sens.*, vol. 12, no. 5, p. 854, Mar. 2020.
[19] I. M. H. Ulander, "Accuracy of using point targets for SAR calibration," *IEEE Trans. Aerosp. Electron. Syst.*, vol. 27, no. 1, pp. 139–148, Jan. 1991.
[20] R. F. Hanssen, "A radar retroreflector device and a method of preparing a radar retroflector device," U.S. Patent 2018236215, Dec. 27, 2018.
[21] J. Groot, "Letter: Cross section computation of trihedral corner reflectors with the geometrical optics approximation," *Eur. Trans. Telecommun.*, vol. 3, no. 6, pp. 637–642, Nov. 1992.
[22] D. Small and A. Schubert, "Guide to sentinel-1 geocoding," Remote Sensing Lab. Univ. Zurich (RSL), Zürich, Switzerland, Tech. Rep. UZH-S1-GC-AD, Mar. 2019.